ELSEVIER

International Journal of Mass Spectrometry 226 (2003) 71–83

International Journal of Mass Spectrometry

www.elsevier.com/locate/ijms

On the formation of initial ion velocities in matrix-assisted laser desorption ionization: Virtual desorption time as an additional parameter describing ion ejection dynamics

Bernhard Spengler*, Dieter Kirsch

Institute of Inorganic and Analytical Chemistry, Justus Liebig University, Schubertstr. 60, D-35392 Giessen, Germany

Received 10 June 2002; accepted 20 June 2002

Abstract

Measurements of initial ion velocities prior to ion acceleration were performed using a special instrumental setup with a variable length of a first field-free stage in a two-stage MALDI ion source. Experimental results showed that drift times through the field-free stage cannot be extrapolated to zero when reducing the length of this stage, but indicate a condition-specific temporal offset. This offset can mathematically be interpreted as a delayed start of ions and is therefore called "virtual desorption time". Mechanistically these virtual desorption times have to be interpreted as being the result of acceleration processes of analyte ions in a molecular jet, leading to various dependencies of analyte ion velocities and virtual desorption times on the chosen experimental parameters, rather than being the result of a delayed desorption of molecular ions or clusters from the surface. Formation of analyte ions by cluster decay is in accordance with the reported observations, as is formation of analyte ions by charge exchange in the gas phase. In both cases, however, the presence of an efficient molecular jet is suggested by these experimental results, leading to a subsequent acceleration of entrained molecular ions after detachment of molecular entities from the solid phase.

Keywords: MALDI; Initial ion velocities; Field-free stage; Molecular jet

1. Introduction

The mechanisms of ion formation and the kinetics of ion ejection in laser desorption ionization (LDI) mass spectrometry have been a matter of fundamental research over quite a long period [1]. Spectral absorption of analyte and/or metallic substrates (targets) [2], acid–base reactions between different components of the sample or between excited and ground-state molecules, and various physico-chemical properties are known to strongly influence the fundamental processes of desorption and ionization. A homogeneous model that could explain all observations on the basis of a set of physico-chemical parameters, however, could not be derived over the years. The situation became even more complex upon the introduction of matrix-assisted laser desorption ionization (MALDI) [3,4], providing for a common behavior of analyte classes and a universal applicability of laser-based

* Corresponding author.
E-mail address: bernhard.spengler@anorg.chemie.uni-giessen.de (B. Spengler).

1387-3806/02/$ – see front matter
PII S1387-3806(02)00974-0

mass spectrometry. Ion–molecule reactions in the gas phase of protonated and/or electronically excited matrix molecules on the one hand and neutral analyte molecules on the other hand, were assumed to dominate the ion formation process [5]. Only very recently an alternative model for ion formation in MALDI was discussed [6], which can be understood as an extension of an earlier model on the formation of ions by cluster decay [7]. Investigation and verification of such models is not a simple approach, since none of the underlying physical quantities are directly measurable. One unique parameter which contains valuable information about the desorption and ionization process is the initial velocity of ions, i.e., the velocity ions acquire or already have, when they leave the target surface and enter the gas phase, prior to an electrostatic acceleration. Ion velocities can be measured through determination of the total kinetic energies of ions, through ion flight times or through flight time variations. These data can give distinct information on the location of ion formation, the time and the momentum of ions after formation.

The translational energy of emitted neutral molecules of high spectral absorption, well below the threshold irradiance of ion formation, was investigated by means of gas-phase photoionization experiments [8–10]. The results of these investigations indicated a thermal desorption model for neutral molecules used as matrices in MALDI-MS. These early experiments were later extended to derive a uniform model for the laser fluence-dependent particle flux [11].

Matrix or analyte ions, in contrast to neutral molecules, do not reveal a quasi-thermal behavior [12,13]. An almost mass-independent initial velocity rather than a mass-independent (i.e., a thermal) kinetic energy of ions was found instead [14–17]. The formation of a molecular jet was therefore postulated as the key mechanism of the desorption step in MALDI [19]. It was concluded that, as in a molecular beam, analyte ions are entrained in a jet of matrix ions and (neutral) molecules, leading to a nearly uniform (mass-independent) velocity.

A new model for ion formation in MALDI was presented recently [6], explaining singly charged, protonated molecular ions observed in MALDI spectra as the “lucky survivors” of a complex, early decay process of multiply charged analyte ions reacting with low-energy photoelectrons. An essential assumption within this model is the formation of initial molecular units from larger units (clusters), leading to highly charged “primary” analyte ions in a process similar to the one suggested for the formation of ions in electrospray ionization (ESI). This cluster decay mechanism was proposed earlier for the formation of alkali attached analyte ions in LDI, but was originally not assumed to be valid for the formation of protonated analyte ions [7]. The latter were thought to be formed by proton exchange reactions between molecular species in the gas phase after laser induced electronic excitation instead [7]. Ion yields, as well as subsequent fragmentation reactions could be explained by an “overlap model” [5], describing protonated analyte molecules as the product of a spatial overlap of protonating matrix ions with neutral analyte molecules in the gas phase.

Ion formation by cluster decay, on the one hand, or by overlap of clouds of ions and neutral molecules, on the other hand, should be accompanied by distinguishable kinetic behavior. Initial kinetic energies should therefore carry informations on the early phase of molecularization and ion formation. In this context, however, the motion of ions after leaving the target surface cannot be regarded as a constant property but has to be monitored as a dynamic parameter evolving in time and space from a complex multi-parameter interaction process.

None of the velocity measurements reported so far [12–17,19,20] take into account the dynamic evolution of the final ejection velocity (“final” here refers to leaving the primary interaction zone, typically prior to an electrostatic ion acceleration). In all of these experiments instead, initial ion velocities were determined from a *single* “late” event or property by extrapolation to the “early” (and assumedly constant) property “initial ion velocity”.

The topic of this paper is to describe the non-constantcy of this early property of ions and to discuss the possible mechanisms of initial velocity formation.

These dynamical effects were investigated by monitoring not just a single late property but a series of those, allowing us to extrapolate the ion velocity evolution in the early phase of ion ejection.

2. Experimental

Initial ion velocities were determined in a two-stage acceleration system of a linear time-of-flight mass spectrometer as described in Fig. 1. The distance between the target and the first electrode was variable between 0.5 and 9 mm, while the length of the 2nd acceleration stage was fixed.

Precise determination of initial velocities requires the precise knowledge and controllability of distances and electrical potentials. Furthermore, fringing fields have to be avoided and all electrostatic fields should be homogeneous. The ion source described in Fig. 1 was especially designed and constructed to fulfill these requirements. It was made sure that all planes of grids, plates and the target were parallel to better than 10 μm. The variable length of the first acceleration stage was controlled by a micrometer stage with a precision of better than 10 μm.

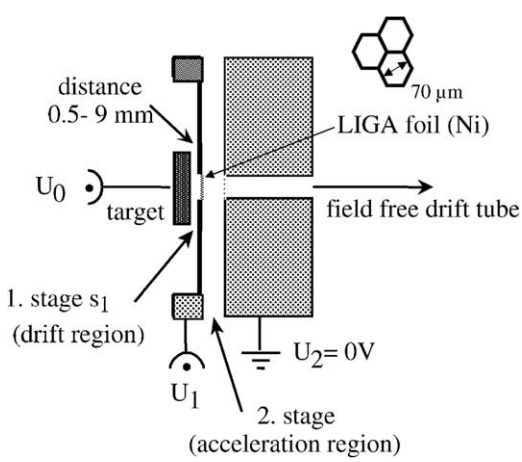

Fig. 1. Scheme of the two-stage acceleration unit for determination of initial velocities of ions. Field penetration into stage 1 was minimized by using a LIGA foil between stages 1 and 2, with a ratio of channel depth to diameter of 0.7.

The main source of errors results from geometrical effects of grids. In precise determination of initial velocities, non-ideal grids can easily lead to errors in the range of several percent, due to fringing fields and field deformation, and dynamical effects cannot be described at all. Instead of using metallic grids we therefore employed etched conductive nickel foils developed especially for this purpose by means of the LIGA technique [21,22]. Similar to the geometry of a microchannel plate, these foils consist of a large number of hexagonal channels with open inner diameters of 70 μm and depths of 50 μm. Only with this arrangement zero field strength in the first stage can be realized at full electrical field strength in the second stage. The geometry of the first electrode was additionally optimized to shield any fringe field from other non-grounded elements of the instrument. The setup was tested for any remaining field penetration as described in Fig. 2. It was found that stage 1 is field free under the chosen experimental conditions.

2.1. Determination of initial velocities

The method of determination of initial velocities in the performed experiments is described in the following: ions passed the first, field-free stage of the ion source before acceleration within the second high-field stage. The total flight time of ions from laser pulse to detection with this setup was compared to the total flight time when using a normal acceleration field in the first stage. Since the final kinetic energy of the ions after leaving the ion source is identical in all cases, the flight time of ions in the field-free region between the second electrode and the detector is identical in both cases. The flight times in the first and second stage, on the other hand, can be calculated and, since distances and potentials are well known, the initial ion velocity can be determined by solving the resulting motion equation.

It is for case 1 (first stage field-free):

$$t_{\text{total}} = t_1(v_{\text{ini}}, s_1) + t_2(v_{\text{ini}}, E_2, s_2, m) + t_{\text{drift}} \qquad (1)$$

and for case 2 (first stage normal acceleration field):

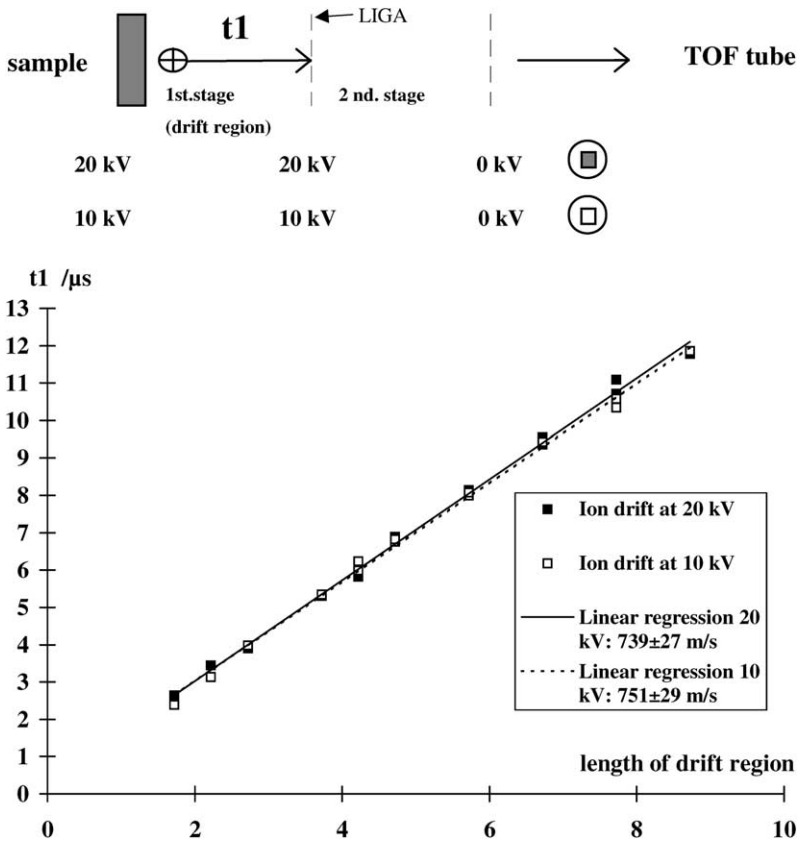

Fig. 2. Setup and result of a field penetration test using melittin as analyte and DHB as a matrix. The electrical field in the first stage was set to zero by applying identical potentials to the sample and the first grid. The electrical field in the second stage was set to different values in order to detect fringing fields. Initial velocities determined with this setup were found to be identical within experimental errors at 10 and 20 kV potentials, indicating that stage 1 is not penetrated by fringing fields from stage 2.

$$t'_{\text{total}} = t'_1(v_{\text{ini}}, s_1, E'_1, m) + t'_2(v'_1, E'_2, s_2, m) + t_{\text{drift}}. \tag{2}$$

Here t_{total} is the total flight time of ions from the desorption to the detection event, t_1 and t_2 the flight times in the first and the second stage, t_{drift} the flight time in the drift region, v_{ini} the initial ion velocity, s_1 and s_2 the lengths of the first and second stage, E_1 and E_2 the electrical field strengths within the first and second stage and m the ion mass.

The determined flight time difference between cases 1 and 2 therefore is

$$\Delta t = t_{\text{total}} - t'_{\text{total}} = t_1 + t_2 - t'_1 - t'_2. \tag{3}$$

The general motion equation for an accelerated motion in an electrical field is:

$$t = \sqrt{m} s_{\text{el}} \sqrt{\frac{2}{|\Delta U|e}} \left[-\text{sgn}(\Delta U)\text{sgn}(v_0) \sqrt{\left|\frac{E_{\text{kin},0}}{\Delta U e}\right|} + \text{sgn}(\Delta U) \sqrt{\left|\frac{E_{\text{kin},0}}{\Delta U e}\right| + \text{sgn}(\Delta U)\frac{s_{\text{flight}}}{s_{\text{el}}}} \right]. \tag{4}$$

Eq. (4) is applicable to any accelerated or decelerated motion with either positive or negative initial velocity. In Eq. (4), t is the flight time within the acceleration or deceleration region, m is the mass, s_{el} is the length of the homogeneous electric field, ΔU is

the potential difference between entry and exit plane of the region, with a positive potential difference corresponding to an acceleration event, e is the elemental charge, sgn is the sign function (positive = 1, negative = −1), v_0 is the initial velocity (velocity upon entry of the resp. region), with a positive value of v_0 corresponding to a drift into the direction of the exit plane, $E_{kin,0}$ is the axial, initial velocity upon entry of the region and s_{flight} is the length of the flight path within the electrical field. Since ions might be formed or might start within the electrical field, s_{el} and s_{flight} are not necessarily identical.

With the initial assumption that all ions start at the same time and at the same place (i.e., on the target surface), Eq. (3) can be calculated as

$$\Delta t = t_1 + t_2 - t_1' - t_2' \tag{5}$$

with

$$t_1 = \frac{s_1}{v_{ini}}, \tag{6}$$

$$t_2 = \sqrt{m} s_2 \sqrt{\frac{2}{|U_2 - U_0|e}} \times \left[-\sqrt{\frac{m v_{ini}^2}{2|U_2 - U_0|e}} + \sqrt{\frac{m v_{ini}^2}{2|U_2 - U_0|e} + 1} \right], \tag{7}$$

$$t_1' = \sqrt{m} s_1 \sqrt{\frac{2}{|U_1 - U_0|e}} \times \left[-\sqrt{\frac{m v_{ini}^2}{2|U_1 - U_0|e}} + \sqrt{\frac{m v_{ini}^2}{2|U_1 - U_0|e} + 1} \right], \tag{8}$$

$$t_2' = \sqrt{m} s_2 \sqrt{\frac{2}{|U_2 - U_1|e}} \times \left[-\sqrt{\frac{E_{kin,1}}{2|U_2 - U_1|e}} + \sqrt{\frac{E_{kin,1}}{2|U_2 - U_1|e} + 1} \right], \tag{9}$$

where

$$E_{kin,1} = \tfrac{1}{2} m v_{ini}^2 + |U_1 - U_0|e. \tag{10}$$

U_0, U_1, U_2 are the potentials of the target, the LIGA foil and the grid as shown in Fig. 1. Eq. (5) cannot be solved in v_{ini} analytically but can easily be approximated numerically.

2.2. Sample preparation

Samples were prepared the normal way, using the dried droplet method. The molar ratio of analyte to matrix was 1:1200. Spectra were recorded from the inner, microcrystalline part of the sample spots, not from the rim of larger matrix crystals, in order to provide for a reproducible and constant plane of ion formation. A nitrogen laser at 337 nm wavelength (model VSL 337 ND, Laser Science Inc., Cambridge, MA, USA) was used for irradiation.

3. Results and discussion

3.1. Mass dependence of initial velocities

Comparison of the initial velocities of different analytes (Fig. 3) shows that, different from an ideal molecular jet, not a complete mass-independence is observed, but a behavior between a jet-like and a thermal ion kinetic. Calculated velocities for an ideal molecular jet (mass-independent velocity) and for a thermal, effusive particle beam (mass-independent kinetic energy) are displayed in Fig. 3 for comparison. The constant kinetic energy of 6.5 eV was chosen by normalization to the observed velocity of substance P.

Table 1 lists the determined ion velocities for 2,5-dihydroxybenzoic acid (DHB) matrix, 1.3 times

Table 1
Initial velocities of analyte ions of various mass

Analyte	Mass (u)	Measured initial velocity (m/s)	Calculated mean initial velocity for thermal ions (m/s)
Substance P	1348	962	962 (normalized)
Melittin	2848	775	664
Insulin	5734	718	468
Lysozyme	14306	691	296

2,5-Dihydroxybenzoic acid was used as a matrix.

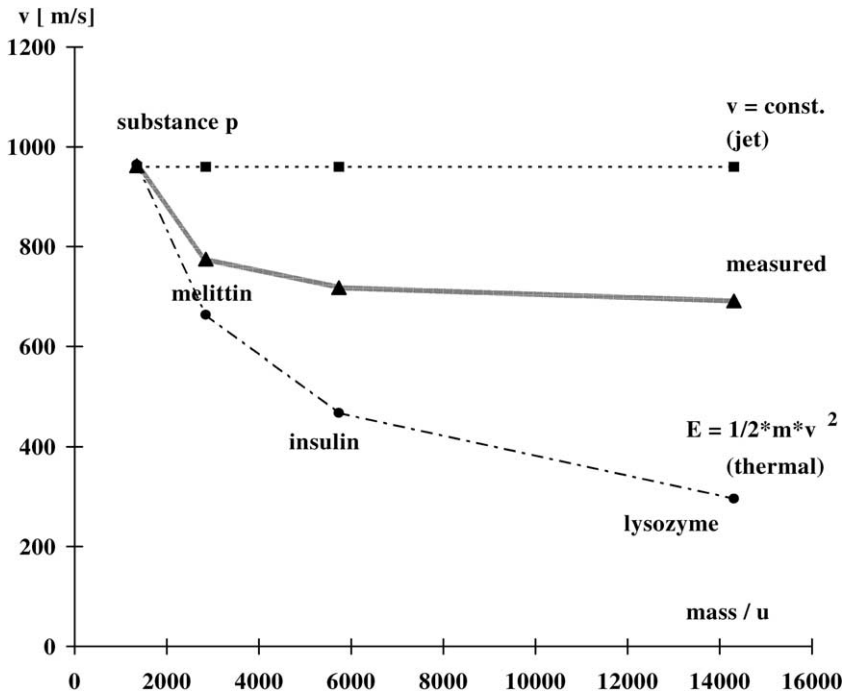

Fig. 3. Mass dependence of ion velocities in an ideal molecular jet, in an effusive (thermal) beam and as measured for MALDI ions in our instrument. DHB was used as a matrix at 1.2 times threshold irradiance. See text for further explanation.

threshold irradiance, 337 nm laser wavelength and a spot size of 25 μm in diameter. It has to be noted that, besides matrix and irradiance, the laser spot size has a considerable influence on the initial ion velocity. Therefore, initial velocities of ions measured on different instruments cannot always be directly compared.

Fig. 3 shows that initial velocities considerably decrease with mass of the analyte ions. The observed effect can be understood taking into account that a MALDI plume ejected by laser irradiation can never be an ideal molecular jet. Due to the pulsed nature of the ejection event, analyte ions cannot be expected to be fully entrained and cooled down to equal axial velocities. It is reasonable instead to expect a reduced but not vanishing mass-dependence of ion velocities, as indeed observed. It is well known that molecular jets must have a minimal duration for a formation of the typical jet characteristics. This minimal duration is typically in the range of almost milliseconds [24,25] and is certainly not obtained in MALDI ejection plumes.

3.2. Irradiance dependence of initial velocities

Different from the results of other groups [26] a significant laser irradiance dependence of ion initial energies was observed in our measurements (Fig. 4). It was found that between the threshold irradiance for ion detection and about twice the threshold irradiance initial ion velocities increase considerably. Above twice the threshold irradiance, ion velocities do not further increase.

It has to be noted that “threshold” is a relative value, connected to the limit of detection of the instrument. It can be assumed that most of the commercial MALDI instruments do not operate under threshold conditions but considerably above this value of irradiance, in order to provide for a constant and sufficiently intense signal for routine operation.

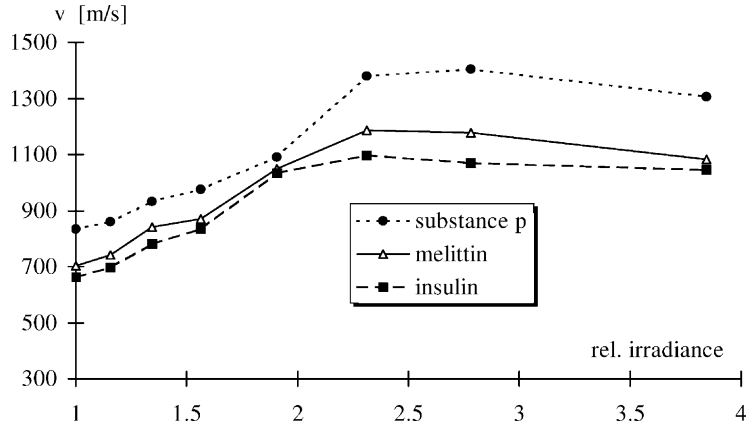

Fig. 4. Initial velocities of substance P, melittin and insulin as a function of the laser irradiance relative to threshold irradiance. DHB was used as a matrix. Initial velocities increase up to about twice the threshold irradiance.

Within the model of molecular jet ejection such behavior can be explained, assuming that particle density increases with irradiance. The majority of these particles are matrix molecules and ions which act as the "carrier gas" in the jet. Acceleration of the (non-ideally entrained) larger analyte ions by collisions with the "carrier gas" (matrix molecules or ions) becomes more efficient with higher particle density. Therefore, analyte ion velocities would increase with particle density, i.e., with laser irradiance, until a final velocity is reached, which is close to the velocity of the carrier gas itself. Due to the pulsed nature of the ejection plume, still a mass dependence of the initial velocities is observed under these conditions (higher irradiance), as seen in Fig. 3, but no longer a particle-density dependence.

An additional confirmation of the jet-like nature of ion ejection is obtained when looking at the drift velocities of the total ion plume, measured at different focus diameters, in a field-free desorption instrument [27]. Increasing the irradiance for a given focus diameter leads to a significant increase of total ion plume velocities [27]. Increasing the focus diameter, on the other hand, results in a lower velocity of ions, when measured at the reduced (focus-specific) threshold irradiance (Fig. 5).

It has to be noted that results from the field-free desorption instrument (Fig. 5) and the two-stage prompt extraction instrument can be compared qualitatively, but not quantitatively. The considerable focus- and irradiance-dependence of the angular distribution of ion ejection has a strong effect on the measurements in the field-free instrument, while it has a negligible effect in the prompt-extraction instrument. The overall observation, however, is obvious in both setups: an increase of ion velocity with increasing irradiance and with decreasing focus diameter. This behavior is in accordance with the model of a pulsed supersonic nozzle beam, where an increase of pressure and a decrease of nozzle diameter leads to an increase of mean particle velocity [27–31].

3.3. Dynamical behavior of initial velocities: virtual desorption times

3.3.1. Matrix dependence of initial velocities

It was observed earlier [23] and is observed in our instrument that employing different matrices results in different initial velocities. In our setup, these initial velocities can be determined for different lengths of the (field-free) first stage of the ion source (Fig. 1). For a uniform motion of ions, the determined values of initial velocity should be identical and independent of the length of the first stage. Fig. 6 shows that the flight times of insulin in the first field-free stage are higher when using α-cyano-4-hydroxycinnamic acid

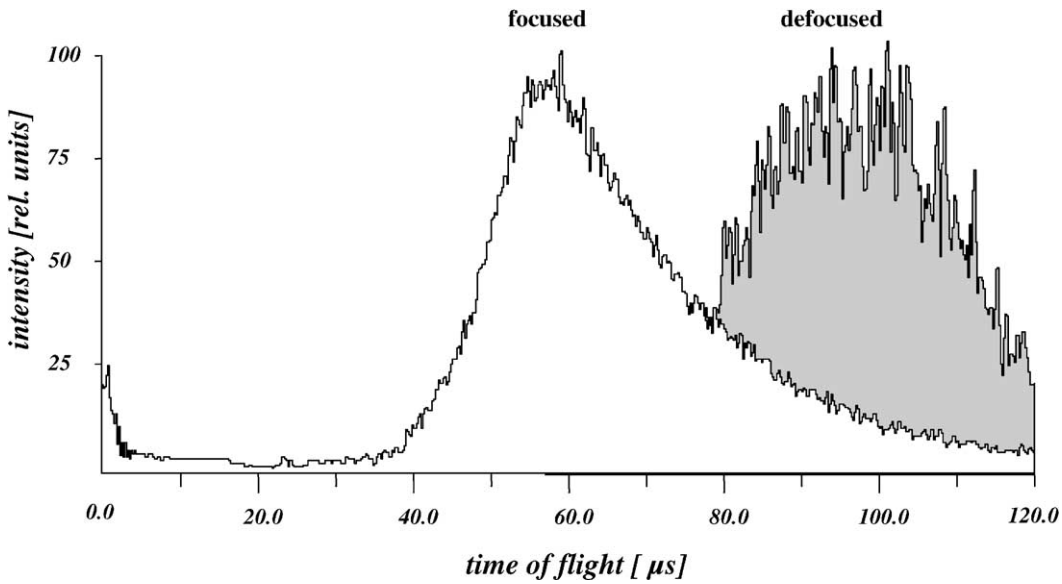

Fig. 5. Flight times of non-accelerated positive ions of DHB through a field-free drift region at 80 μm focus diameter ("focused") and at 150 μm focus diameter ("defocused") at various relative laser irradiances. The absolute threshold irradiance is lower for defocused conditions than for focused conditions.

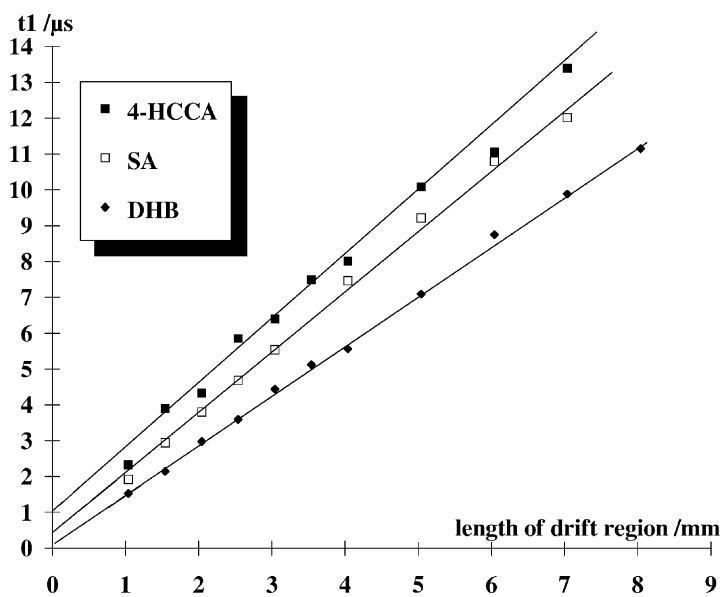

Fig. 6. Flight times of insulin ions in the field-free drift region s_1 of various length using different matrices. The irradiance used was 1.4 times threshold irradiance. Determined velocities and virtual desorption times are listed in Table 2.

Table 2
Initial velocities (slopes) and virtual desorption times of insulin ions

Matrix	Velocity (m/s)	Virtual desorption time (μs)
4-HCCA	571	1.0
Sinapinic acid	583	0.3
DHB	717	0.1

(4-HCCA) as a matrix than when using sinapinic acid or DHB as a matrix, as expected. An unexpected observation, however, is that extrapolation of the flight times in the field-free first stage to zero length of this stage does not lead to zero flight times but to matrix-specific positive values in time. These time values can formally be described as "virtual desorption times" or "virtual moments of desorption" since the determined drift times through the first stage suggest a "late start" of ions (relative to the time of the laser pulse). The extrapolated virtual desorption times of insulin ions in 4-HCCA, sinapinic acid and DHB are 1.0, 0.3 and 0.1 μs, respectively (Table 2).

Table 3
Initial velocities (slopes) and virtual desorption times of insulin ions

Relative irradiance (E/E_0)	Velocity (m/s)	Virtual desorption time (μs)
1.2	694 ± 18	+0.23 ± 0.1
3.1	840 ± 27	−0.05 ± 0.1

Observation of non-zero virtual desorption times is not an artifact of the experimental setup but a systematic event, as is further confirmed by looking at the stage-length dependent drift times of analyte ions as a function of laser irradiance (Fig. 7). While virtual desorption times of insulin ions reach zero (within experimental errors) at high laser irradiance, they are in the range of 0.2 μs at threshold irradiance (Table 3).

The formation of non-zero virtual desorption times can be interpreted in three alternative ways:

1. Analyte ions are desorbed late from the sample surface, with a constant initial velocity.

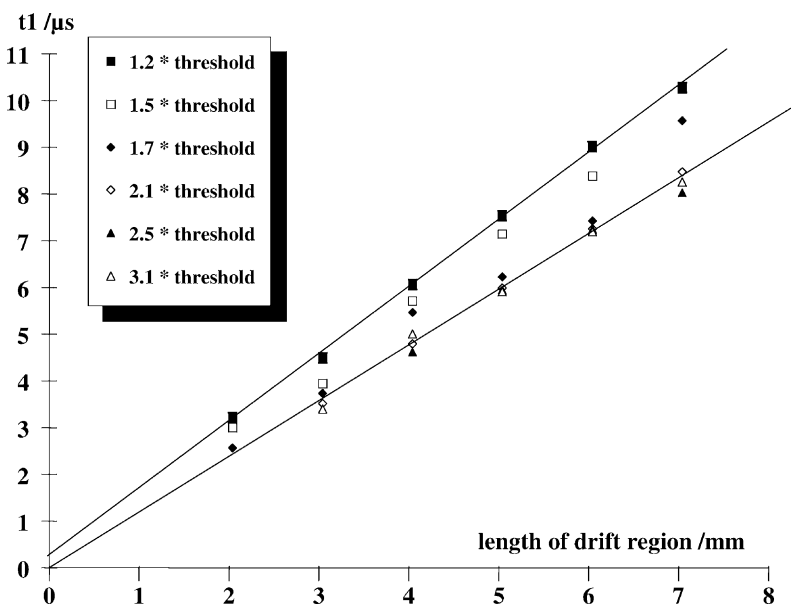

Fig. 7. Flight times of insulin ions in the field-free drift region s_1 of various length at various laser irradiances. The matrix used was 2,5-dihydroxybenzoic acid. Determined velocities and virtual desorption times are listed in Table 3. The focus diameter was 25 μm in diameter.

2. Analyte molecules are desorbed from the surface and are ionized in the gas phase, or analyte ions are desorbed as pre-formed ions from the surface. Both obtain their initial velocity by collisions with matrix molecules or ions in the jet.
3. Analyte ions are formed from ejected and moving larger clusters (cluster decay model [6,7]) and are accelerated afterwards by collisions with matrix molecules and ions.

A fourth model would be a pure cluster decay model, where ions are formed from moving clusters without further interaction within a molecular jet. This cluster model is basically proposed by molecular modelling calculations [18], where no considerable velocity difference between clusters and molecular species is assumed.

The first interpretation (late desorption) is certainly the most straightforward one, but it is, on the other hand, quite hard to explain, why different matrices should lead to different delays in ion desorption, and why desorption at threshold irradiance should lead to delays of up to microseconds, while desorption at high irradiances leads to immediate desorption.

The second interpretation is much more consistent with other observations and with well-known physical effects. The model for the formation of virtual desorption times by gas-phase collisions in a pulsed jet is summarized in Fig. 8.

Analyte ions or neutral analyte molecules are desorbed from the surface with thermal velocities, according to this model. Acceleration of these slow molecular species by collisions with faster entities (matrix molecules or ions) within the pulsed MALDI jet will be finalized as earlier as higher the particle density of the “carrier gas” (the matrix plume) is. At the same time, with higher particle densities and thus larger number of collisions, the final velocity of analyte molecules or ions will be closer to the velocity of the carrier gas. A low collision rate therefore will lead to a slow acceleration process, to a low final velocity and to a late virtual desorption time (upper curve). A high collision rate, on the other hand, will lead to a fast acceleration process, a high final velocity and to early virtual desorption times.

It is in this model irrelevant, whether ionization takes place in the sample or in the gas-phase since

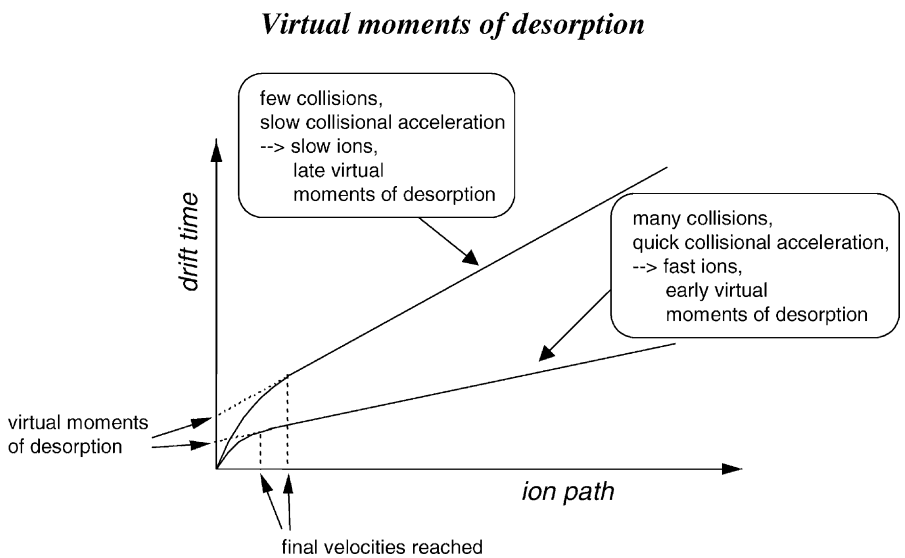

Fig. 8. Model for the formation of positive virtual desorption times.

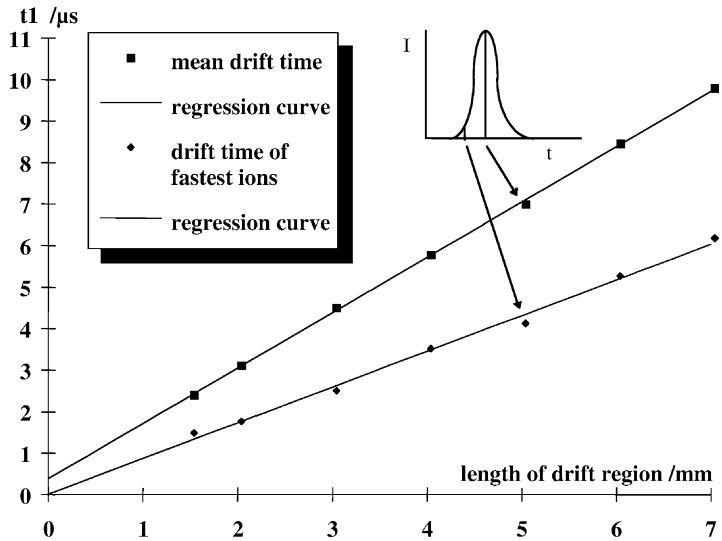

Fig. 9. Flight times of negative oligonucleotide ions TTGAC in the field-free drift region s_1 using DHB as a matrix. Mean velocities and velocities of the fastest ions at 10% signal height were determined from each ion signal. Determined velocities and virtual desorption times are listed in Table 4.

the postulated acceleration processes take place in a field-free environment.

Another indication for collisional acceleration as the underlying process leading to virtual desorption times is obtained from analysis of ions of different velocities from the same ion package. Assuming that in a linear time-of-flight instrument with electrostatic (not pulsed) acceleration fields, ions with the highest initial velocity will appear first at the detector, one is able to discriminate ion packets with different initial velocities by evaluation of the corresponding sections of an ion signal (Fig. 9) (Table 4).

Ions from the center of an ion package, again, show significant values of virtual desorption times, as expected from the measurements on peptide ions. The leading ions of an ion package, however, have virtual desorption times very close to zero (i.e., close to the laser pulse time). This again indicates that ions with high initial velocities are those who have suffered a large number of accelerating collisions and who therefore have reached their final velocity very early.

Table 4
Initial velocities (slopes) and virtual desorption times of negative TTGAC ions using DHB as a matrix

Species	Velocity (m/s)	Virtual desorption time (µs)
Mean velocity	750 ± 20	+0.4 ± 0.1
Fastest ion package	1164 ± 27	+0.02 ± 0.1

4. Conclusion

A set of observations has to be tested versus different models of ion formation and desorption. Table 5 summarizes the observations described in this paper and their consistencies with the four models of ion formation and desorption.

The results described in this paper suggest that ions are not ejected from the sample surface by a thermal mechanism nor are they released from clusters into an interaction-free vacuum. The observed virtual desorption times, irradiance dependences and mass dependences can only be interpreted as being the result of acceleration processes after release of analyte molecules from either the sample surface or from clusters, into an energetic molecular jet which imprints

Table 5
Summary of observations and their consistencies with various desorption and ionization models

Observation	Model 1: late start (thermal model)	Model 2: molecular jet (acceleration effects)	Model 3: cluster decay + molecular jet (acceleration effects)	Model 4: pure cluster decay (no further acceleration after ion formation)
Mass dependence (Fig. 3)	≠[a]	√	√	≠[a]
Irradiance dependence of initial velocities (Fig. 4)	≠[b]	√	√	≠[b]
Focus dependence (Fig. 5)	≠[c]	√	√	√[h]
Matrix dependence (Fig. 6)	≠[a]	√	√	≠[a]
Irradiance dependence of virtual desorption times (Fig. 7)	≠[a]	√[e]	√	≠[i]
Fast/slow ion packages (Fig. 9)	√[d]	√[f]	√[g]	≠[j]

(√): consistent with model; (≠): contradiction to model.
[a] No explanation for observed behavior.
[b] No explanation why velocity increases only up to two times threshold irradiance.
[c] Thermal desorption should not be focus-dependent.
[d] Thermal behavior with early and late desorption events.
[e] Acceleration effect (particle density).
[f] Acceleration effect.
[g] Early and late release of ions from clusters with subsequent acceleration.
[h] Assuming that ejected clusters have higher velocity at smaller focus diameters.
[i] No explanation for virtual desorption times as a function of irradiance.
[j] No explanation for virtual desorption times as a function of velocity.

an "initial" velocity onto the analyte molecules. It cannot be decided, whether analyte molecules and ions are entrained into the molecular jet at the very beginning of the desorption event (model 2) or whether molecular ions are entrained into a jet after formation from slow clusters and subsequently accelerated by the jet (model 3; cluster decay model with molecular jet formation). It can, however, be excluded that the MALDI process is solely a process of ejection of larger clusters evaporating thermally into molecular entities. In this case, analyte ions formed from these clusters would not be accelerated further but would continue to move with the initial velocity of the ejected clusters. No acceleration effects would be observed then, i.e., the determined virtual desorption times should be equal to zero in this case.

A simple, late ejection of clusters, as an alternative way to explain virtual desorption times besides a subsequent jet acceleration of molecular ions formed, cannot explain the observed effects either. If clusters would be ejected with a certain (matrix-specific) delay, one should not observe different virtual desorption times for the fast and the slow part of ions within an ion package (Fig. 9), but ions would move on with the initial velocity of the clusters (with a certain process-specific velocity distribution). Even with assuming a certain distribution of cluster desorption times there would still be no correlation between analyte ion velocities and virtual desorption times of anlyte ions.

The main conclusion of the above measurements therefore is, that the MALDI process must be dominated by a molecular jet behavior. That means that the majority of material (primarily matrix material) is ejected as molecules and molecular ions and only a small part might be ejected as clusters, susceptible to decay and "cluster-induced" ion formation. Only under these conditions of a dense molecular jet, ions formed from cluster decay can further be accelerated and form a temporal behavior as observed in our measurements, including non-zero "virtual desorption times".

It cannot be excluded from the above observations that both general processes of analyte ion formation, cluster decay on the one hand and gas-phase protonation of analyte molecules by protonated matrix

molecular ions on the other hand, take place in parallel in MALDI. Formation of two modes of analyte ions would be the consequence of such a dual-process mechanism. One would then expect to obtain rather different analyte ion velocities and different virtual desorption times for the two modes of ion formation. With the current set of data available from our or other experiments this question cannot be addressed and remains open.

Acknowledgements

Financial support by the Deutsche Forschungsgemeinschaft (Sp 314/3-1,2) is gratefully acknowledged.

References

[1] F. Hillenkamp, U. Bahr, M. Karas, B. Spengler, Scanning Microsc. Suppl. 1 (1987) 33.
[2] M. Karas, D. Bachmann, F. Hillenkamp, Anal. Chem. 57 (1985) 2935.
[3] M. Karas, D. Bachmann, U. Bahr, F. Hillenkamp, Int. J. Mass Spectrom. Ion Process. 78 (1987) 53.
[4] M. Karas, F. Hillenkamp, Anal. Chem. 60 (1988) 2299.
[5] V. Bökelmann, B. Spengler, R. Kaufmann, Mass Spectrom. 1 (1995) 81.
[6] M. Karas, M. Glückmann, J. Schäfer, J. Mass Spectrom. 35 (2000) 1.
[7] B. Spengler, U. Bahr, M. Karas, F. Hillenkamp, J. Phys. Chem. 91 (1987) 6502.
[8] B. Spengler, U. Bahr, M. Karas, F. Hillenkamp, Anal. Instrum. 17 (1988) 173.
[9] B. Spengler, U. Bahr, F. Hillenkamp, in: T.B. Lucatorto, J.E. Parks (Eds.), Resonance Ionization Spectroscopy 1988, The Institute of Physics Conference Series No. 94, Bristol, 1988, p. 307.
[10] B. Spengler, U. Bahr, F. Hillenkamp, in: T.B. Lucatorto, J.E. Parks (Eds.), Resonance Ionization Spectroscopy 1988, The Institute of Physics Conference Series No. 94, Bristol, 1988, p. 137.
[11] K. Dreisewerd, M. Schürenberg, M. Karas, F. Hillenkamp, Int. J. Mass Spectrom. Ion Process. 141 (1995) 127.
[12] B. Spengler, J. Dolce, Y. Pan, R.J. Cotter, in: Proceedings of the 2nd International Symposium on Applied Mass Spectrometry in the Health and Life Sciences, Barcelona, 17–20 April, 1990.
[13] B. Spengler, R.J. Cotter, Anal. Chem. 62 (1990) 793.
[14] Y. Pan, R.J. Cotter, Org. Mass Spectrom. 27 (1992) 3.
[15] R.C. Beavis, B.T. Chait, Chem. Phys. Lett. 181 (1991) 479.
[16] T. Huth-Fehre, C.H. Becker, Rapid Commun. Mass Spectrom. 5 (1991) 378.
[17] W. Ens, Y. Mao, F. Mayer, K.G. Standing, Rapid Commun. Mass Spectrom. 5 (1991) 117.
[18] L.V. Zhigilei, B.J. Garrison, Rapid Commun. Mass Spectrom. 12 (1998) 1273.
[19] R.C. Beavis, B.T. Chait, Chem. Phys. Lett. 181 (1991) 479.
[20] P. Juhasz, M.L. Vestal, S.A. Martin, J. Am. Soc. Mass Spectrom. 8 (1997) 209.
[21] P. Bley, Interdiscipl. Sci. Rev. 18 (1993) 267.
[22] B.Y. Cheng Y, M.K. Chyu, Nucl. Instrum. Meth. A 467 (2001) 1192.
[23] M. Glueckmann, M. Karas, J. Mass Spectrom. 34 (1999) 467.
[24] K.L. Saenger, J. Chem. Phys. 75 (1981) 2467.
[25] K.L. Saenger, J.B. Fenn, J. Chem. Phys. 79 (1983) 6043.
[26] A. Verentchikov, W. Ens, J. Martens, K.G. Standing, Experimental study of ion ejection processes in matrix-assisted laser desorption, in: The 40th ASMS Conference on Mass Spectrom and Allied Topics, 1992, p. 360.
[27] B. Spengler, V. Bökelmann, Nucl. Instrum. Meth. Phys. Res. B82 (1993) 379.
[28] J.B. Anderson, in: P.P. Wegener (Ed.), Molecular Beams and Low Density Gas Dynamics, Dekker, New York, 1974.
[29] J.B. Anderson, R.P. Andres, J.B. Fenn, Advances in Chemical Physics, vol. 10, p. 275.
[30] J.B. Anderson, J.B. Fenn, Phys. Fluids 8 (5) (1965) 780.
[31] N.F. Ramsey, Molecular Beams, vol. 10, Clarendon Press, Oxford, 1956.